Controlled Voltage Breakdown in Disconnector Contact System for VFTO mitigation in Gas-Insulated Switchgear (GIS)

Marcin Szewczyk, *Senior Member, IEEE*, Maciej Kuniewski, *Member, IEEE*

***Abstract*— Several methods have been proposed and investigated so far on mitigation of Very Fast Transient Overvoltages (VFTO) in Gas-Insulated Switchgear (GIS). The state-of-the-art methods are primarily based on dissipation of the energy associated with electromagnetic waves that the VFTO originate from and are composed of. Present paper reports on an alternative concept of VFTO mitigation based on the principle of controlling voltage conditions preceding voltage breakdown in SF_6 gas that leads to VFTO generation. The paper introduces different control algorithms and shows how the algorithms can limit VFTO maximum value and total number of voltage breakdowns during operation of the GIS disconnector. The concept is applied for mitigation of VFTO in ultra-high voltage (UHV) GIS. As the study case, an 1'100 kV test set-up is used as recently reported for Wuhan (China) GIS station, with the disconnector characteristics obtained from 1'100 kV development tests.**

***Index Terms*— Very Fast Transient Overvoltages (VFTOs), Gas-Insulated Switchgear (GIS), disconnector switch (DS), transients, switching, mitigation, controlled breakdown**

I. Introduction

VERY Fast Transient Overvoltages (VFTO) originate from voltage breakdowns in SF_6 gas that inherently accompany any operation of Gas-Insulated Switchgear (GIS) disconnector [1]. The VFTO process is characterized mainly by the VFTO peak value, frequency of its main components, and the number of occurrences during the disconnector opening or closing operations. The frequency components of VFTO are related to the time duration of the voltage breakdown in SF_6 gas and to the travelling wave conditions along the GIS. The VFTO peak values result from the voltage conditions at the time instance just preceding of the voltage breakdown (spark ignition) and to the travelling wave conditions along the GIS as well [2]. Fig. 1 presents an example of VFTO waveform obtained from development tests of 1'100 kV disconnector.

Analysis and mitigation techniques related to VFTO attract high attention among industry and academia, specifically in recent years when the power grid faces the advent of extra-high voltage (EHV) and ultra-high voltage (UHV) class GIS. For these high voltage levels the VFTO peak values can exceed the GIS insulation withstand voltage and thus can become a design factor of the GIS components [3]. It implies that the VFTO generated during the disconnector operations needs to be accurately investigated to ensure proper design of the GIS components and to support a decision making process on the potential application of VFTO mitigation techniques. In some GIS solutions the VFTO needs to be mitigated in order to maintain the VFTO peak values within the limits that are acceptable for a specific design of components.

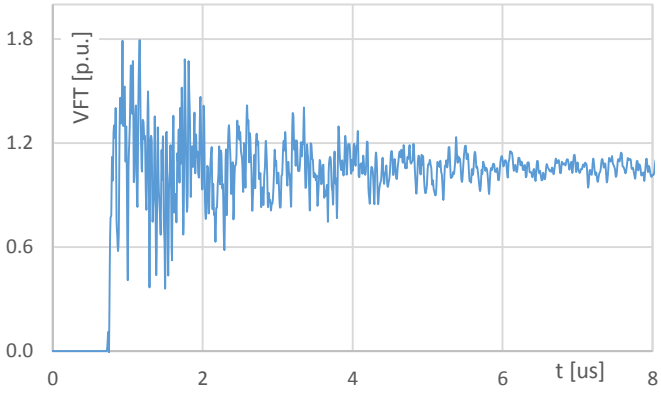

Fig. 1 Example of, VFTO waveform obtained from development tests of 1'100 kV GIS disconnector (1 p.u. = $V_r \cdot \sqrt{2}/\sqrt{3}$, V_r – rated voltage)

A. Methods of VFTO attenuation

Several methods have been proposed so far for mitigation of VFTO originating from the GIS disconnector operations. Also, review works, such as [4] and [5], have been published, giving an overview of the state-of-the-art methods. The state-of-the-art methods of VFTO mitigation include disconnector equipped with a resistor inserted in the disconnector contact system [6], and application of magnetic rings of different types (ferrite [7], [8], [9], amorphous [10], or nanocrystalline [9], [11], [12], [13]) in the GIS busducts. With respect to the methods based on the energy dissipation in the magnetic materials, recently a new magnetic material was proposed and tested for VFTO attenuation as reported in [14]. The recently published new methods include also resonators with a sparking element, with the resonance frequencies that are fitted to the main VFTO

M. Szewczyk is with ABB Corporate Research Center, 31-038 Krakow, Starowislna 13A, Poland (e-mail: marcin.szewczyk@pl.abb.com).

M. Kuniewski is with AGH University of Science and Technology, Department of Electrical and Power Engineering, al. Mickiewicza 30, 30-059 Kraków, Poland (e-mail: maciej.kuniewski@agh.edu.pl).

Corresponding author: M. Szewczyk (e-mail: marcin.szewczyk@pl.abb.com).

Color versions of one or more of the figures in this paper are available online at http://ieeexplore.ieee.org

components [15], the GIS busbars equipped with surge arresters [16], and the disconnector with a new arrangement of the contact system [17]. All of these methods are based on a common principle of attenuation of the energy associated with the electromagnetic waves that constitute or have constituted the VFTO.

A state-of-the-art method on VFTO mitigation that to some extent involves controlling of the voltage conditions that precede the voltage breakdowns in the disconnector contact system, is based on reducing the voltage associated with the trapped charge (the so-called trapped charge voltage, TCV) that remains at the load-side of the disconnector after the opening operation is completed [4], [18], [19]. The most severe voltage conditions for the disconnector type testing are defined in [20], for the first voltage breakdown during the closing operation for the TCV = -1.1 p.u. (where 1 p.u. = $V_r \cdot \sqrt{2}/\sqrt{3}$; V_r – rated voltage). According to [4], [18], [19], the TCV can be controlled by proper disconnector design. The most common design changes that are reported for controlling of the TCV are related to the disconnector moving contact speed.

B. Controlling of voltage ignition in switching devices

It is known from previous works in the subject that the voltage breakdown can be controlled in a switching device. Applications of selected techniques of voltage breakdown control have already been implemented in MV switching devices in vacuum [21]. One of the solutions is to introduce a trigger electrode into the contact system of the vacuum interrupter chamber to initiate additional voltage flashovers between the contacts at the assumed time instances. Also, triggered spark gaps are in use for dielectric tests of HV insulation to conduct tests with voltage impulse chopped at any time instance on the front or on the tail [22]. This method is also used in HV trigatrons, for which specific operating characteristics are discussed in [23] as dependent upon the detailed construction of the device.

Different phenomena are recognized as potentially useful to ignite a voltage breakdown in the contact system of the switching device. Experiments with laser-triggered electrical breakdown with a proposal of different triggering electrode configurations are reported for gases [24] and for liquids [25]. The voltage breakdowns induced by microwaves are reported in [26].

C. Paper overview

This paper presents a concept of VFTO mitigation by means of controlling voltage conditions that precede the voltage breakdowns in the GIS disconnector contact system. The analysis is presented of the VFTO mitigation for different control algorithms applied to 1'100 kV test set-up as recently reported for the Wuhan (China) GIS station [27]. The Wuhan test set-up has been thoroughly described in [19], [27], [28], [29], [30], and the disconnector design-specific characteristics has been recently described in [27]. In the present paper we outline the test set-up briefly and focus on the VFTO mitigation analysis with the use of the proposed control algorithms.

The paper is organized as follows: Section I gives the overview of the state-of-the-art methods of VFTO mitigation in GIS. It shows how the new method that we propose in the present paper fits to the previously published works in the subject. Techniques of controlling voltage breakdown in gases and vacuum are outlined and medium-voltage application of these techniques is indicated. Section II presents the VFTO generation process and the control algorithms that we analyze in the present paper. Section III describes the test-set-up used for VFTO analyses. Section IV reports on the results of simulations of the VFTO distributions and the total number of voltage breakdowns during the disconnector closing operation. Section V offers conclusions.

II. Concept Description: VFTO Mitigation by Controlled Voltage Breakdown in Disconnector Contact System

A. VFTO generation process with no control algorithm

To illustrate the concept presented in this paper, in this section we assume a simplified simulation case with an illustrative, simplified Breakdown Voltage Characteristics (BDV) of the GIS disconnector. The BDV characterizes the disconnector dielectric strength at any time instance of the disconnector operation and it is strongly dependent on the disconnector design (insulation distances, design of shielding elements, contact system design, gas pressure) as well as on the travelling curve of the disconnector moving contact. In Section IV we applied the control algorithms presented in the present Section II for the test set-up described in Section III.

Fig. 2 illustrates the disconnector opening (see Fig. 2a) and closing (see Fig. 2b) operations, with the opening time of 0.12 s and the voltage withstand of 3.5 p.u. for the fully opened contacts, with no control algorithm employed. For simulation of the disconnector operation process, we employed the method that is thoroughly described in [28]. Along the present paper, the disconnector source-side 50 Hz voltage u_S is depicted in green color, the disconnector load-side step-wise voltage u_L is depicted in blue color, and the BDV characteristics are depicted in red or brown colors.

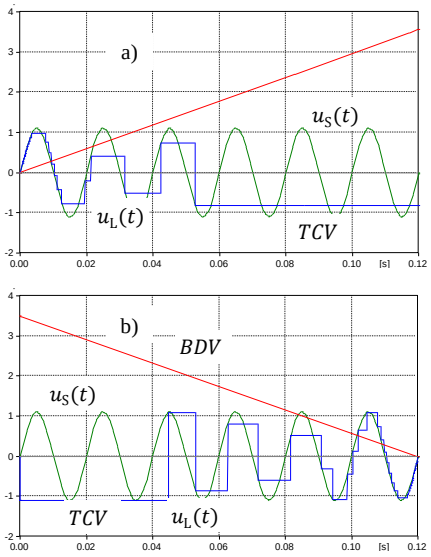

Fig. 2 Voltage waveforms illustrating disconnector opening (a) and closing (b) operations with simplified Breakdown Voltage Characteristics assumed; u_S – disconnector source-side 50 Hz voltage, u_L – disconnector load-side step-wise voltage, BDV – Breakdown Voltage Characteristics, TCV – Trapped Charge Voltage.

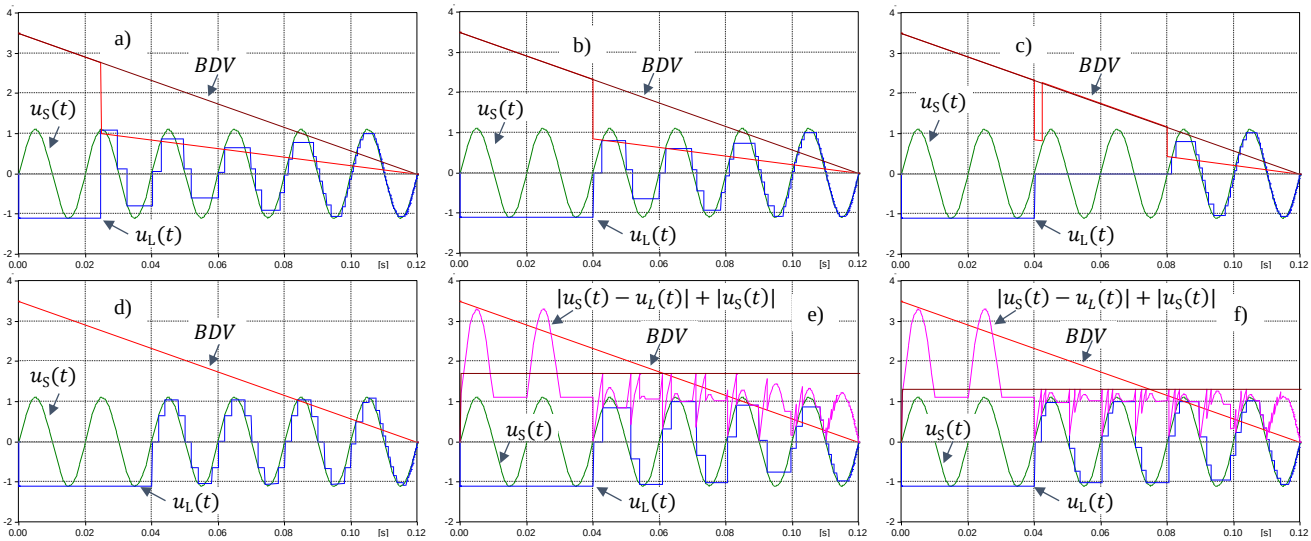

Fig. 3 Voltage waveforms illustrating disconnector closing operation with different control algorithms employed for controlling voltage breakdown ignitions; a) BDV modification, b) BDV modification starting from zero u_S, c) BDV modification starting from zero u_S then released and then again modified, d) voltage breakdown ignitions at fixed time intervals, e) voltage breakdowns initiated according to (1) with A_{const} = 1.7 p.u., f) voltage breakdowns initiated according to (1) with A_{const} = 1.3 p.u.; u_S, u_L, BDV – same notation used as in Fig. 2

For the illustrative process shown in Fig. 2, only few voltage breakdowns (spark ignitions) occur. It can be noticed that the trapped charge voltage (TCV) at the disconnector load-side, that remains after opening operation is completed (see Fig. 2a) have significant value, however lower than the maximum possible value of -1.1 p.u. Through design modifications of the disconnector the TCV can be controlled to maintain its level as significantly lower than the maximum possible -1.1 p.u. [4], [18].

Fig. 2b illustrates closing operation for the same parameters as used for the opening operation shown in Fig. 2a, also with no control algorithm employed. Here, the worst-case scenario is assumed for the TCV, i.e. TCV = -1.1 p.u., which is in compliance with IEC recommendations for type testing [20]. The assumption of TCV = -1.1 p.u. remains unchanged in the subsequent simulations reported in the following sections.

The first voltage breakdown during the closing operation (see Fig. 2b) occurs in the maximum (amplitude) value of the source-side 50 Hz voltage u_S. This reproduces the real disconnector behavior, where the BDV decreases significantly slower as compare to the 50 Hz variation of the source side voltage u_S.

For both operations shown in Fig. 2, the last occurrence of the voltage breakdown for the opening operation (see Fig. 2a) and the first one for the closing operation (see Fig. 2b) are observed for the highest voltage difference at the disconnector contact system (thus producing the highest VFTO, not shown in the figures). The subsequent voltage breakdowns occur for significant, however lower and decreasing voltage values.

B. *Control algorithms*

Fig. 3 illustrates a set of control algorithms that are discussed in the present Section II for the purpose to illustrate the concept presented in this paper. The algorithms shown in Fig. 3 are then applied in Section III for simulation of VFTO in a real 1'100 kV test set-up. All of the simulations shown in Fig. 2 (no control algorithms, reference case) and in Fig. 3 (control algorithms) were performed for the same voltage conditions and for the same starting time of the disconnector operation process (phase angle of the source-side voltage u_S at the disconnector operation start).

The control algorithms shown in Fig. 3 are of two principle types. Fig. 3a,b,c show the algorithms where the BDV is modified for selected time ranges (which causes that the voltage breakdowns occur at different time instances than in the reference case where no algorithm is employed), while Fig. 3d,e,f show the algorithms where the voltage breakdowns are initiated at given time instances (depending on the time and voltage conditions).

In the subsequent paragraphs, a description of each of the algorithms illustrated in Fig. 3 is given. The algorithms are grouped according to the data that is required to be available as an input for the algorithm realization (source side 50 Hz voltage u_S and/or load side voltage u_L).

The performance of each of the algorithms also relies on the prior knowledge of the disconnector BDV characteristics (which is dependent on particular disconnector design and can be determined based on the disconnector development or type tests as reported in [27]). Thus, each of the control algorithms discussed below has two principle versions: with or without prior knowledge of the disconnector BDV.

1) Input data: u_S – not available, u_L – not available

Fig. 3a shows the control algorithm where none of the voltages are measured and no prior knowledge on the disconnector BDV is available. The BDV is modified at a randomly selected time instance and kept at lower level until the end of the disconnector closing operation process. For illustration purposes, the simulation parameters are selected so that the first voltage breakdown occurs at the time instance of the maximum value of the source-side voltage u_S, i.e. for the

highest possible voltage across the disconnector contact system (worst-case scenario). Even for this worst case scenario, the subsequent voltage breakdowns occur for the decreased voltages as compare to the reference case with no modified BDV (as shown in Fig. 2b), leading to lower subsequent VFTO.

Modification of the BDV in a way shown in Fig 3a leads to increased number of voltage breakdowns as compare to the no-control reference case shown in Fig. 2b (as the sparks are being ignited earlier and more frequently in the process), however with lower VFTO values.

2) Input data: u_S – available, u_L – not available

Fig. 3b shows a similar algorithm as the one shown in Fig. 3a and discussed above. The only difference is that now the BDV modification starts from the time instance of the source-side voltage u_S zero crossing. This ensures that the first VFTO occurs with significantly decreased voltage across the disconnector contact system as compared to the worst-case scenario shown in Fig. 3a. The time instance when the BDV modification starts is selected so that the first voltage breakdown occurs prior to the time instance when the voltage breakdowns would have started with no control algorithm employed.

Fig. 3c shows further modification of the algorithms shown in Fig. 3a and Fig. 3b. The BDV is modified starting from the same time instance as for the algorithm shown in Fig. 3b. This causes that the load-side voltage u_L is reduced to approximately zero value at the first voltage breakdown. Then, after the subsequent zero crossing of the source-side voltage u_S, the BDV is released to its normal condition, and yet again the BDV is modified at one of the subsequent zero crossings of u_S. The second BDV modification can favorably be done for the zero crossing of u_S just before the time instance when the ignitions would start anyway for the normal BDV conditions.

This algorithm allows for lower number of voltage breakdowns as compare to the algorithm shown in Fig. 3b (as the BDV is now not modified when the sparks would not have occurred anyway).

Fig. 3d shows a different algorithm as compared to the ones previously described. Here, the voltage breakdowns are ignited at the time intervals of fixed length. The time intervals are short enough to ensure that the voltage across the contact system for any of the voltage breakdown is sufficiently low. The algorithm starts at the time instance of the source-side voltage u_S zero crossing that precedes the time instance when the voltage breakdowns would have occurred in the case when the BDV would not be controlled.

3) Input data: u_S – available, u_L – available

Fig. 3e and Fig. 3f show the control algorithm for which the voltage breakdowns are ignited when the following condition is met:

$$|u_S(t) - u_L(t)| + |u_S(t)| = A(t) < A_{const} \qquad (1)$$

where $u_S(t)$ – is the disconnector source-side 50/60 Hz voltage, $u_L(t)$ – is the disconnector load-side voltage, $A(t)$ is a function of voltage across the contact system $|u_S(t) - u_L(t)|$ superimposed on the instantaneous value of the source-side voltage $u_S(t)$; A_{const} is a pre-assumed constant value to which the $A(t)$ is compared.

According to (1), the voltage breakdowns are ignited when the voltage across the disconnector contact system superimposed on the instantaneous value of the source-side voltage exceeds the pre-assumed constant value A_{const}. As the VFTO forms around the u_S, the formula (1) allows to control the voltage conditions preceding voltage breakdown that leads to VFTO generation. To represent different voltage conditions, Fig. 3e and Fig. 3f illustrate the algorithms for A_{const} = 1.7 p.u. and A_{const} = 1.3 p.u. respectively. For the case with A_{const} = 1.3 p.u. the VFTO peak values are expected to be lower and the number of sparks higher than for the case with A_{const} = 1.7 p.u.

C. Summary on control algorithms

It can be seen in Fig. 3 that application of any control algorithm presented leads to lower voltage across the disconnector contact system and thus to lower expected VFTO values. As the voltage breakdowns occur at lower voltage conditions, higher number of voltage breakdowns are expected.

When the BDV is known from prior-tests, the start of the control algorithm can be properly selected, to avoid voltage breakdowns at relatively high voltage conditions and at the same time to minimize number of additional voltage breakdowns introduced to the process. This should take into account statistical variation of the BDV as well as a possible inaccuracy of the control timing. Igniting the voltage breakdowns at the time instance of the source-side voltage u_S zero crossing allows to avoid high voltage across the disconnector contact at the time of the spark ignition, thus minimizing the corresponding VFTO. Without prior knowledge of BDV, the algorithms can be used as well, however risking that the first voltage breakdown occurs at the most severe source-side voltage u_S conditions (as shown in Fig. 3a).

III. Test set-up for VFTO analyses

This section outlines the GIS test set-up layout and the disconnector BDV characteristics assumed for the VFTO analyses reported in Section IV.

A. Test set-up layout and parameters

Fig. 4 shows the test set-up established in 2009 by State Grid Corporation China (SGCC) in Wuhan 1'100 kV GIS station in China and used in the present paper. Several research works have been published so far based on the outcome of the measurements obtained in this test set-up (e.g. [19], [28], [29], [30], and most recently [27]), presenting analyses of different aspects of VFTO generation process in UHV GIS. In the present paper we modeled the Wuhan test set-up based on the principle rules published in e.g. [31], [32] and for the layout parameters published in [29], [30].

B. Disconnector Breakdown Voltage Characteristics (BDV)

Fig. 5 shows the BDV determined in [27] based on the full-scale measurements conducted for an 1'100 kV disconnector as used by ABB at development tests (see Fig. 5 in [27]). In the present paper, we implemented this characteristics in the model of the test set-up of Wuhan station as shown in Fig. 4. As the BDV shown in Fig. 5 is non-symmetrical, in the simulations we

assumed the negative branch as serving for the lower voltage withstand in terms of the absolute voltage values (thus leading to higher expected VFTO).

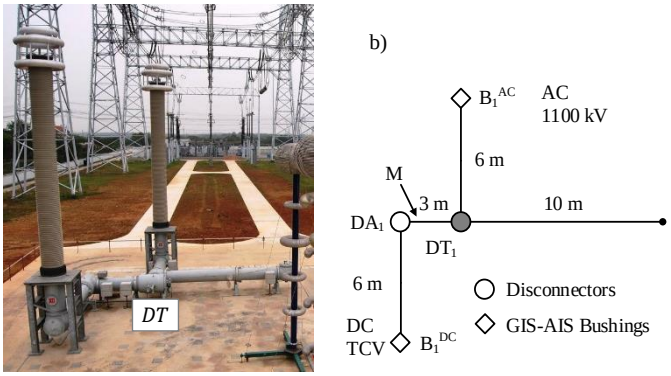

Fig. 4 Test set-up of Wuhan 1'100 kV GIS station according to [29], [30]; lengths assumed in Section IV for simulations; measuring point *M* corresponds to *M1* in [27]; *DT* – disconnector under test, the picture is reproduced here from [28] © 2013 IEEE, and the diagram is reproduced here from [27] © 2016 IEEE.

In Fig. 5 the time instances of the BDV crossing ±2.2 p.u. and ±2.4 p.u. are indicated. The ±2.2 p.u. is the lowest BDV, for which the voltage breakdowns can occur. The value of -2.4 p.u. was assumed in the present paper as the value beginning from which the control algorithm starts to initiates voltage breakdowns.

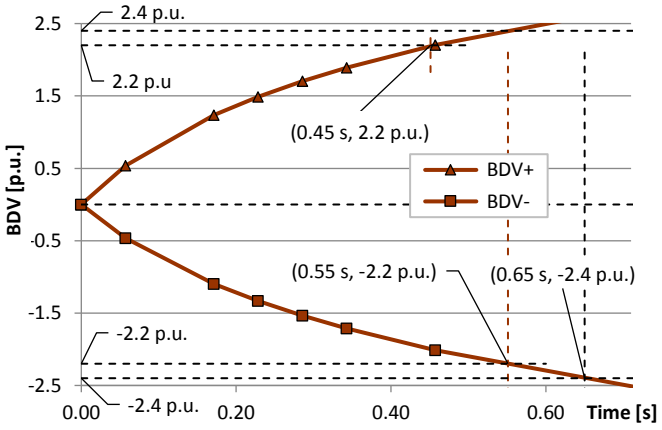

Fig. 5 Breakdown Voltage Characteristics of 1'100 kV disconnector obtained in development tests BDV as reported in [27] (see Fig. 7 in [27]); maximum possible arcing times can occur for 2.2 p.u. (marked as 0.49 ms for positive- and 0.55 ms for negative BDV).

IV. Simulation Results for 1'100 kV GIS with Different Control Algorithms of Voltage Breakdown

Simulation results presented in this section were performed for the Wuhan 1'100 kV test set-up as shown in Fig. 4, and for the 1'100 kV disconnector for which the measured BDV characteristics is shown in Fig. 5 [27]. The control algorithms were used as illustrated in Fig. 3. Each of the algorithm was applied for the closing operation, for which the VFTO distributions as well as the total number of sparks occurring in the operation process were calculated. For each of the simulation case, the control algorithm started for the condition when the absolute value of BDV decreased below 2.4 p.u. to ensure that the spontaneous breakdowns (without any algorithm employed) will not occur before the algorithm starts.

Following the work presented in [27], the VFTO were calculated for selected location within the test set-up, denoted as *M* in Fig. 4.

A. Simulation results for VFTO distributions

Fig. 6 shows simulation results of VFTO distributions for four simulation cases: with no control algorithm as shown in Fig. 3a (see Fig. 6a), for the control algorithm with the modified BDV as shown in Fig. 3c (see Fig. 6b), for the control algorithm with the spark ignitions at fixed time intervals of 2.5 ms as shown in Fig. 3d (see Fig. 6c), and for the control algorithm where the sparks are ignited according to (1) as shown in Fig. 3e,f (see Fig. 6d).

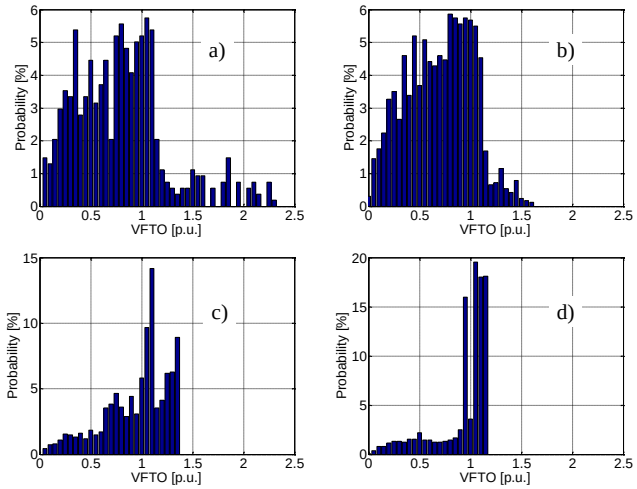

Fig. 6 Distributions of VFTO obtained for point *M* in test set-up shown in Fig. 4, for closing operations of disconnector BDV shown in Fig. 5, for the control algorithms illustrated in Fig. 3: a) No control, b) BDV modified as per Fig.3c, c) Sparks ignited in equal time intervals 25 ms as per Fig. 3d, d) Sparks ignited according to A(t) as per Fig. 3e,f with A_{const} = 1.1 p.u.

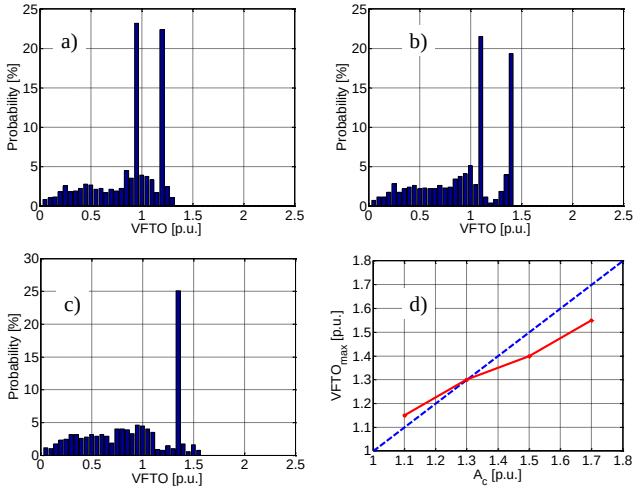

Fig. 7 Distributions of VFTO obtained for point *M* in test set-up shown in Fig. 4, for closing operations of disconnector BDV shown in Fig. 5, for the control algorithm illustrated in Fig. 3e,f where sparks are ignited according to A(t) with: a) A_{const} = 1.3 p.u., b) A_{const} = 1.5 p.u., c) A_{const} = 1.7 p.u., d) A_{const} = (1.1, 1.3, 1.5, 1.7) p.u.

The maximum value of the VFTO ($VFTO_{max}$) simulated for the no control reference case can be read out from Fig. 6a as 2.3 p.u., which is in agreement with the corresponding value in [27] and with the measurement results reported in [28] for the same simulation conditions (see text below Table IV in [27]).

Fig. 7a,b,c show distributions of VFTO for the same conditions as for Fig. 6, with the control algorithm in which the sparks are ignited according to formula (1) as shown in Fig. 3e,f. Different values of Aconst are assumed. Fig. 7d shows the maximum VFTO values (VFTOmax) obtained for each of the Aconst assumed (from Fig. 6d and Fig. 7a,b,c), showing the increase of VFTOmax with the increase of the Aconst parameter.

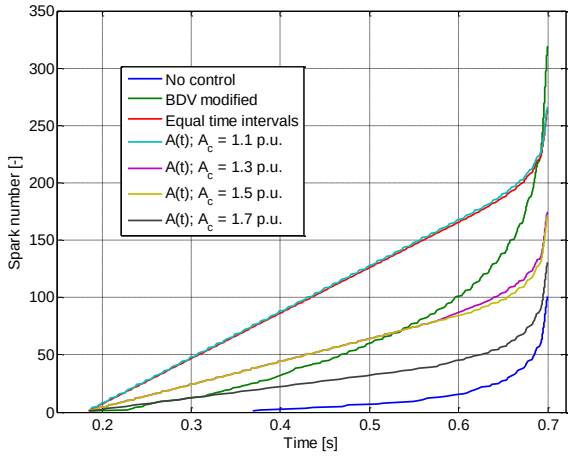

Fig. 8 Number of sparks obtained for point *M* in test set-up shown in Fig. 4, for closing operation of disconnector BDV shown in Fig. 5, for the control algorithms illustrated in Fig. 3.

TABLE I
Summary of simulation results shown in Fig. 6-8; $VFTO_{max}$ is the maximum value obtained in the VFTO distributions in Fig. 6-7, n_{max} is the total number of voltage breakdowns occurring in the process.

Algorithm (see Fig. 3)	***VFTO*max [p.u.] (see Fig. 6, 7)**	***n*max [-] (see Fig. 8)**
No control (see Fig. 3a)	2.30	101
BDV modified (see Fig. 3c)	1.60	319
Equal time intervals (see Fig. 3d)	1.35	264
A(t) < A_{const} = 1.1 p.u. (see Fig. 3e,f)	1.15	266
A(t) < A_{const} = 1.3 p.u. (see Fig. 3e,f)	1.30	174
A(t) < A_{const} = 1.5 p.u. (see Fig. 3e,f)	1.40	172
A(t) < A_{const} = 1.7 p.u. (see Fig. 3e,f)	1.55	131

B. Simulation results for number of sparks

Fig. 8 shows the total number of sparks ignited in a single closing operation process, for the same control algorithms as previously applied and shown in Fig. 6 and Fig. 7.

Table I summarizes the $VFTO_{max}$ (as shown in Fig. 6 and Fig. 7) and of the total number of sparks (as shown in Fig. 8) for each of the algorithm employed (as illustrated in Fig. 3). It can be seen that by selection of the voltage breakdown control algorithm, the $VFTO_{max}$ and the number of sparks in the process can be controlled. Decreased $VFTO_{max}$ leads to increase of the number of voltage breakdowns in the proces (see Table I, row 1 vs. rows 2-7). This can be further controlled by proper selection of the control algorithm parameters (see Table I, rows 4-7).

V. Conclusions

Currently, high attention among industry and academia is given to investigation of methods for attenuation of Very Fast Transient Overvoltages (VFTO) in Gas-Insulated Switchgear (GIS), specifically for EHV and UHV class GIS. Most of the state-of-the-art methods are based on the energy dissipation of the electromagnetic waves associated with VFTO.

A novel concept was presented in this paper by means of which the VFTO mitigation is achieved by controlling of the voltage conditions preceding voltage breakdowns in the disconnector contact system. Examples of control algorithms are presented, firstly for an illustrative simulation case, and then applied for the real 1'100 kV test set-up. The analysis of the control algorithms impact on the VFTO mitigation process was performed for a model of 1'100 kV Wuhan GIS station in China with the Breakdown Voltage Characteristics of 1'100 kV disconnector obtained from development tests reported in [27].

It has been shown that by controlling the voltage conditions at which the voltage breakdowns occur during the disconnector operation process, the VFTO as well as the number of voltage breakdowns can be controlled. With the control algorithms presented, limiting of the VFTO peak values causes an increased number of the voltage breakdowns at the same time. The control algorithms presented in this paper assume full control over the time instances of the voltage breakdowns.

The work presented can serve as a base for development of the GIS disconnector with a voltage breakdown control system. As the voltage breakdown characteristics is dependent upon the detailed construction of the GIS disconnector, final evaluation should be performed for specific design of the GIS disconnector contact system. The application of the control algorithms presented can then lead to more optimized design of the disconnector and more reliable substation solution.

VI. References

[1] G. Ecklin and D. Schlicht, "Overvoltages in GIS caused by the operation of isolators," in *Proc. 1979 of the Brown Boveri Research Centre*, Baden, Switzerland, September 3-4, 1979.

[2] M. Szewczyk, K. Kutorasiński, M. Wroński, M. Florkowski, "Full-Maxwell Simulations of Very Fast Transients in GIS: Case Study to Compare 3D and 2D-Axisymmetric Models of 1100 kV Test Set-Up," *IEEE Trans. Power Delivery* [accepted for publication, available in IEEEXplore, DOI: 10.1109/TPWRD.2016.2527823], Feb. 2016.

[3] Working Group C4.306, Insulation Coordination for UHV AC Systems, *CIGRE Technical Brochure 542*, June 2013.

[4] U. Riechert, M. Bösch, M. Szewczyk, W. Piasecki, J. Smajic, A. Shoory, S. Burow, S. Tenbohlen, "Mitigation of Very Fast Transient Overvoltages in Gas Insulated UHV Substations", 44th CIGRÉ Session, 2012.

[5] A. Tavakoli, A. Gholami, H. Nouri, M. Negnevitsky, "Comparison between suppressing approaches of Very Fast Transients in Gas-Insulated Substations (GIS)," *IEEE Trans. Power Delivery*, vol. 28, no 1, pp. 303-310, Jan. 2013.

[6] Y. Yamagata, K. Tanaka, S. Nishiwaki, N. Takahashi, T. Kokumai, I. Miwa, T. Komukai, K. Imai, "Suppression of VFT in 1100 kV GIS by adopting resistor-fitted disconnector," *IEEE Tran. Power Delivery*, vol. 1, no 2, pp. 872-880, April 1996.

[7] W. D. Liu, L. J. Jin, J. L. Qian, "Simulation test of suppressing VFT in GIS by ferrite rings," in Proc. 2001 International Symposium on Electrical Insulating Materials, pp. 245-247, Beijing, China, 2011.

[8] J. V. G. Rama Rao, J. Amarnath, S. Kamakshaiah, "Simulation and measurement of Very Fast Transient Overvoltages in a 245 kV GIS and research on suppressing method using ferrite rings," ARPN Journal of Engineering and Applied Sciences, vol. 5, no 5, pp. 88-95, May 2010.

[9] S. Burow, U. Riechert, W. Köhler, S. Tenbohlen, "New mitigation methods for transient overvoltages in gas insulated substations," in Proc. Stuttgarter Hochspannungssymposium, Stuttgart, Germany, 2012, pp. 169-181.

[10] Y. Guan, G. Yue, W. Chen, Z. Li, W. Liu, "Experimental Research on Suppressing VFTO in GIS by Magnetic Rings," *IEEE Trans. Power Delivery*, vol. 28, No. 4, pp. 2558-2565, Oct 2013.

[11] S. Burow, U. Straumann, W. Köhler, S. Tenbohlen, "New Methods of Damping Very Fast Transient Overvoltages in Gas-Insulated Switchgear," *IEEE Trans. Power Delivery*, vol. 29, No. 5, pp. 2332-2339, October 2014.

[12] M. Szewczyk, J. Pawłowski, K. Kutorasiński, W. Piasecki, M. Florkowski, U. Straumann, "High-Frequency Model of Magnetic Rings for Simulation of VFTO Damping in Gas-Insulated Switchgear With Full-Scale Validation," *IEEE Trans. Power Delivery*, vol. 30, No. 5, pp. 2331-2338, October 2015.

[13] M. Szewczyk, K. Kutorasiński, J. Pawłowski, W. Piasecki, M. Florkowski, "Advanced Modeling of Magnetic Cores for Damping of High-Frequency Power System Transients," *IEEE Trans. on Power Delivery*, vol. 31, no. 5, pp. 2431-2439, Apr. 2016.

[14] M. Szewczyk, W. Piasecki, M. Stosur, M. Florkowski, U. Riechert, "Damping of VFTO in Gas-Insulated Switchgear by a New Coating Material," *IEEE Trans. Power Delivery*, vol. 31, No. 6, pp. 2553-2558, Feb. 2016.

[15] J. Smajic, A. Shoory, S. Burow, W. Holaus, U. Riechert, S. Tenbohlen, "Simulation-Based Design of HF Resonators for Damping Very Fast Transients in GIS," *IEEE Trans. Power Delivery*, 2014.

[16] S. Burow, U. Straumann, W. Köhler, S. Tenbohlen, "New Methods of Damping Very Fast Transient Overvoltages in Gas-Insulated Switchgear," *IEEE Trans. Power Delivery*, vol. 29, No. 5, pp. 2332-2339, October 2014.

[17] M. Szewczyk, W. Piasecki, M. Wroński, K. Kutorasiński, "New concept for VFTO attenuation in GIS with modified disconnector contact system," *IEEE Trans. Power Delivery*, vol. 30, No. 5, pp. 2138-2145, October 2015.

[18] Szewczyk M., Piasecki W., Stosur M., Riechert U., Kostovic J., "Impact of Disconnector Design on Very Fast Transient Overvoltages in Gas-Insulated UHV Switchgear", Proceedings of 17th International Symposium on High Voltage Engineering (ISH), August 22nd-26th, Hannover, Germany, 2011.

[19] S. Yinbiao, H. Bin, L. Ji-Ming, C. Weijiang, B. Liangeng, X. Zutao, C. Guoqiang, "Influence of the Switching Speed of the Disconnector on Very Fast Transient Overvoltage," *IEEE Trans. Power Delivery*, vol. 28, No. 4, pp. 2080-2084, October 2013.

[20] *High-Voltage Switchgear and Controlgear—Part 102: Alternating Current Disconnectors and Earthing Switches*, IEC 62271-102.

[21] F. Gai, S. Chen, H. Jiang, W. Tian, J. Chen, X. Li, "Analysis of Conduction Characteristics of Field-Breakdown Triggered Vacuum Switches," *IEEE Trans. Plasma Science*, vol. 41, no. 8, pp. 2160-2165, August 2013.

[22] J. L. Parpal, H. P. Mercure and G. R. Mitchel, "Laser Triggered Chopped Wave Generator," *IEEE Trans. on Power Delivery*, vol. 2, no. 4, pp. 1141-1144, Oct. 1987.

[23] E. Kuffel, W. S. Zaengl, J. Kuffel, "High Voltage Engineering – Fundamentals," 2nd Edition, Newnes 2000

[24] R. A. Dougal, P F Williams, "Fundamental processes in laser-triggered electrical breakdown of gases," *Journal of Physics D: Applied Physics*, vol. 17, No. 5, p. 903, 1984.

[25] A. Sunesson, P. Barmann, S. Kroll, L. Walfridsson, "Laser triggering of electric breakdown in liquids," *IEEE Trans. Dielectrics and Electrical Insulation*, vol. 1, no. 4, pp. 680-691, August 1994.

[26] B. M. Song, D. A. Hammer, C. Golkowski, Yong-Lai Tian, "Initiation of microwave-induced electrical breakdown of high-pressure gases," *IEEE Trans. Plasma Science*, vol. 31, no. 1, pp. 146-156, February 2003.

[27] M. Szewczyk, M. Kuniewski, W. Piasecki, M. Florkowski "Determination of Breakdown Voltage Characteristics of 1'100 kV disconnector for modeling of VFTO in Gas-Insulated Switchgear," *IEEE Trans. Power Delivery*, vol. 31, No. 5, pp. 2151-2158, Dec. 2015.

[28] Y. Shu, W. Chen, Z. Li, M. Dai, Ch. Li, W. Liu, and X. Yan, "Experimental Research on Very-Fast Transient Overvoltage in 1100-kV Gas-Insulated Switchgear," *IEEE Trans. Power Delivery*, vol. 28, no. 1, pp. 458-466, Jan. 2013.

[29] Y. Gongchang, L. Weidong, Ch. Weijiang, G. Yonggang, and L. Zhibing, "Development of Full Frequency Bandwidth Measurement of VFTO in UHV GIS," *IEEE Trans. Power Delivery*, vol. 28, no. 4, pp. 2550-2557, Oct. 2013.

[30] W. Chen, H. Wang, B. Han, L. Wang, G. Ma, G. Yue, Z. Li, and H. Hu, "Study on influence of Disconnector Characteristics on Very Fast Transient Overvoltage in 1100 kV Gas-Insulated Switchgear," to be published.

[31] D. Povh, H. Schmitt, O. Volcker, R. Witzmann, P. Chewdhuri, A. E. Imece, R. Iravani, J. A. Martinez, A. Keri, A. Sarshar, "Modeling and Analysis Guidelines for Very Fast Transients," *IEEE Power Engineering Review*, vol. 17, issue 13, 1996.

[32] M. Szewczyk, M. Stosur, W. Piasecki, M. Kuniewski, P. Balcerek, M. Florkowski, U. Riechert, "Measurements and Simulations of Very Fast Transients during Disconnector," Przegląd Elektrotechniczny, 2012, vol. 88, issue 11B.

VII. BIOGRAPHIES

Marcin Szewczyk (M'2012–SM'2014), born in Koszalin, Poland, received his M.Sc. and Ph.D. degrees in Electrical Engineering from Warsaw University of Technology, Warsaw, Poland, in 2000 and 2009 respectively. He was Assistant Professor at Warsaw University of Technology. Since 2010 he is a Researcher with ABB Corporate Research in Cracow, Poland. His research is mainly in the field of power system analyses and advanced simulations, power products, transients analyses and transients mitigation, insulation coordination, 3D modeling and simulations of electromagnetic fields, modeling of magnetic materials for transient analyses, modeling of Vacuum Circuit Breakers. Dr. Szewczyk is a member of IEEE and Polish Society for Theoretical and Applied Electrical Engineering (ABB Corporate Research, Starowiślna 13A, 31-038 Krakow, Poland, E-mail: marcin.szewczyk@pl.abb.com).

Maciej Kuniewski (Student'11–M'14), born in Kraków, Poland, in 1986. He received his Ph.D. in Electrical Engineering in 2013 from AGH University of Science and Technology in Kraków. He is working as research assistant at AGH in Electrical Engineering and Electrical Power Engineering Faculty. His fields of studies are High Voltage Engineering, transients in power system, overvoltage protection, computer simulations. Maciej Kuniewski is member of IEEE and CIGRE.